The Effect of the Dynamic Wet Troposphere on VLBI Measurements

R. N. Treuhaft and G. E. Lanyi
Tracking Systems and Applications Section

Calculations using a statistical model of water vapor fluctuations yield the effect of the dynamic wet troposphere on Very Long Baseline Interferometry (VLBI) measurements. The statistical model arises from two primary assumptions: (1) the spatial structure of refractivity fluctuations can be closely approximated by elementary (Kolmogorov) turbulence theory, and (2) temporal fluctuations are caused by spatial patterns which are moved over a site by the wind. The consequences of these assumptions are outlined for the VLBI delay and delay rate observables. For example, wet troposphere induced rms delays for Deep Space Network (DSN) VLBI at 20-deg elevation are about 3 cm of delay per observation, which is smaller, on the average, than other known error sources in the current DSN VLBI data set. At 20-deg elevation for 200-s time intervals, water vapor induces approximately 1.5×10^{-13} s/s in the Allan standard deviation of interferometric delay, which is a measure of the delay rate observable error. In contrast to the delay error, the delay rate measurement error is dominated by water vapor fluctuations. Water vapor-induced VLBI parameter errors and correlations are calculated. For the DSN, baseline length parameter errors due to water vapor fluctuations are in the range of 3–5 cm. The above physical assumptions also lead to a method for including the water vapor fluctuations in the parameter estimation procedure, which is used to extract baseline and source information from the VLBI observables.

I. Introduction

Very Long Baseline Interferometry (VLBI) measures the differential phase of an electromagnetic wave between two antennas on the Earth's surface. Typically the waves originate from compact extragalactic radio sources, such as quasars. The inferred group delay, which is the primary VLBI observable, reflects the distance between the two antennas as well as the angle between the vector connecting the antennas and the vector pointing to the radio source (Refs. 1, 2, and 3). In establishing a radio reference frame of radio source and baseline coordinates for navigation, delays other than the geometric delay are regarded as errors in the VLBI measurement. The presence of atmospheric water vapor along the lines of sight from each antenna to the source will affect the index of refraction of the traversed medium, and will therefore corrupt the geometric delay measurement (Ref. 4). The rate of change of the phase delay over few-minute time scales, which is the other principal observable of VLBI, will also be affected by water vapor (Ref. 5).

Parameters estimated from the group delay and phase delay rate observables will in turn suffer errors due to the fluctuating water vapor, or wet troposphere. Typical estimated parameters include baseline length, baseline orientation radio source positions, clock offsets, and zenith troposphere delays (Refs. 6 and 7). In most intercontinental VLBI data reduction, zenith troposphere delay parameters are statistically estimated. This technique essentially accounts for a spatially and temporally average troposphere, for each station, for the time over which the zenith parameter is estimated. The wet troposphere fluctuations around these averages are the dominant tropospheric errors, which map to errors in VLBI astrometric and geodetic parameters.

When centimeter-level VLBI observable accuracies are required, the deviations from a temporally and spatially constant wet troposphere must be considered. This article therefore concentrates on the fluctuations in the wet troposphere delay, which cannot be removed as an error source by the VLBI zenith parameter estimation. While the external calibration technique of using water vapor radiometers (WVRs) (Ref. 8) can largely remove the water vapor-induced radiometric error, understanding the character and effect of the fluctuating wet delay is important. Such an understanding will help to evaluate errors in data which are not accompanied by WVR measurements, which constitute almost all of the DSN VLBI data set as well as most VLBI data taken at other institutions. Due to the low elevation limit of 20 deg for current WVRs, direct, external calibration of the low elevation angle observations necessary in intercontinental VLBI will remain impossible. The analysis of such observations will benefit from a statistical description of tropospheric fluctuations at low elevations. This report is also motivated by the need to assess how WVRs can be used to the best advantage when they are available.

We quantify the effect of the wet troposphere by first describing a statistical model of spatial and temporal tropospheric fluctuations in Section II. In Section III the magnitude of the effect indicated by the statistical model on the VLBI delay and delay rate observables is explored. Evidence of the effects of tropospheric fluctuation from the DSN VLBI data set is also shown. Section IV describes a general procedure for calculating the average VLBI parameter errors induced by the wet troposphere. Errors induced in the baseline length parameter are derived as an example of the general error calculation. Section IV also outlines a method for including the statistical description of the troposphere in the VLBI estimation procedure to obtain improved parameter estimates and parameter covariances. Comparisons of model results with data and other calculations are shown in Section V on model validation. In Section VI, we present conclusions and plans for future experimental and analytical approaches to the problem of wet delay fluctuations.

II. A Statistical Model of Water Vapor Fluctuations

There are two principal assumptions in the statistical model developed below: (1) the spatial structure of index of refraction fluctuations can be closely approximated by elementary (Kolmogorov) turbulence theory, and (2) temporal fluctuations are caused by spatial patterns which are moved over a site by the wind. To simplify model calculations, we will further assume that the water vapor spatial structure as well as the wind vector is independent of height up to an effective height to be discussed at the end of this section. Unless otherwise noted, we will also assume that this finite slab of atmospheric water vapor moves across a flat Earth. The model will be described below, and the results of the calculations will be compared to some of the existing data in Section V.

In describing the spatial statistics of the wet troposphere, we will frequently use a quantity called the structure function. For a random function $f(\vec{r})$, where $\vec{r}$ is a vector in space, the structure function for a displacement vector $\vec{R}$ is defined as (Ref. 9):

$$D_f(\vec{r}, \vec{R}) = \langle (f(\vec{r} + \vec{R}) - f(\vec{r}))^2 \rangle \qquad (1)$$

where the $\langle\,\rangle$ brackets mean ensemble average. The fundamental randomly varying function to be considered will be the refractivity $n(\vec{r})$ as a function of the spatial coordinate $\vec{r}$.[1] Following Ref. 9, we will assume that its structure function is homogeneous and isotropic, that is, that $D_n(\vec{r}, \vec{R})$ is a function of $|\vec{R}| = R$ only, and that it has the form

$$D_n(R) = \langle (n(\vec{r} + \vec{R}) - n(\vec{r}))^2 \rangle = C^2 R^{2/3} \qquad (2)$$

where C in Eq. (2) characterizes the ensemble or the "rockiness" of the spatial inhomogeneity. In most of our applications, we assume that C does not vary with $\vec{r}$ or $\vec{R}$. The consequences of this assumption will be discussed in Section V. It will be shown in the next section that an average C can be determined from WVR data or from the VLBI data itself. Equation (2) is the principal assumption of Kolmogorov turbulence, which is generally derived from dimensional considerations (Refs. 9 and 10). For the refractivity function $n(\vec{r})$, ensemble averaging means considering the behavior of this function for a set of possible tropospheric spatial patterns.

An important random function in calculations which follow is the delay experienced by an electromagnetic wave as it passes through the turbulent atmosphere,

[1] Throughout this article, refractivity is represented by n (refractivity = index of refraction −1). Note that n in the literature is more commonly used for the index of refraction.

$$\tau_{\theta,\phi}(\vec{x}) = (1/\sin\theta)\int_0^h dz\, n(\vec{x} + \vec{r}(\theta, \phi, z))$$

The vector $\vec{r}$ is along the direction described by the elevation and azimuth θ and ϕ with vertical projection z. The coordinate $\vec{x}$ represents an observation site on the surface of Earth, and h is the effective height of the wet troposphere. The ensemble averaged, squared difference between the delay for two antennas separated by a vector $\vec{\rho}$ on the Earth's surface is the structure function of the delay

$$D_{\tau,\theta,\phi}(\rho) = \langle(\tau_{\theta,\phi}(\vec{x} + \vec{\rho}) - \tau_{\theta,\phi}(\vec{x}))^2\rangle \qquad (3)$$

where each antenna is looking along a ray with elevation θ and azimuth ϕ. The expression for $D_{\tau,\theta,\phi}(\rho)$ in terms of $D_n(R)$ can be calculated by integrating through the finite atmosphere the time delay of a signal as it approaches Earth. Extending the derivation of Ref. 9 yields

$$D_{\tau,\theta,\phi}(\rho) = (1/\sin\theta)^2 \int_0^h \int_0^h D_n\left(\left[\rho^2 + 2(z - z')\rho\cot\theta\cos\phi + \frac{(z - z')^2}{\sin^2\theta}\right]^{1/2}\right) dz\, dz'$$

$$- (1/\sin\theta)^2 \int_0^h \int_0^h D_n(|z - z'|/\sin\theta)\, dz\, dz' \qquad (4)$$

In Eq. (4), h is taken to be the effective height of the wet troposphere. Equation (4) is the general expression for the structure function of signals arriving at antennas separated by a distance ρ. The azimuth ϕ is relative to the line connecting the two antennas. Equation (4) is derived in Appendix A.

We have numerically integrated Eq. (4) as a function of ρ for two geometrical cases: $\theta = 90°$ and $(\theta, \phi) = (20°, 45°)$, and the result is shown in Fig. 1 versus $\alpha = \rho/h$. $D_{\tau,\theta,\phi}(\rho)$ was normalized to $C^2\, h^{8/3}$, since only the shape of the curve in Fig. 1 is important for now. The novel result of Fig. 1 is that $D_{\tau,\theta,\phi}(\rho)$ is not a strict power law. It is often assumed (e.g., Ref. 9) that $\rho \ll h$, which yields the result that $D_{\tau,\theta,\phi}(\rho) \propto \rho^{5/3}$ and power functions are frequently used to describe the spatial structure function. In most of the applications that follow, $\rho \geq h$. The result of integrating Eq. (4) without restrictions on the size of ρ relative to h demonstrates that the structure function behaves as $\rho^{5/3}$ at small ρ and as $\rho^{2/3}$ at large ρ, and changes continuously between those two limits. This important result will surface repeatedly in calculations of rms scatters and Allan variances, both of which are usually considered to be power functions of time, but in this picture deviate from power law in a fashion analogous to the deviation in Fig. 1.

Another feature of Fig. 1, which will be common to many of the calculations which follow, is the elevation dependence of the structure function. At small antenna separations, the structure function is roughly proportional to the tropospheric path length. We use the phrase "path length" to mean the effective distance traveled by a wave from the top of the wet troposphere to an antenna; it is approximately proportional to (sin (elevation angle))$^{-1}$. As the distance ρ becomes many times the wet troposphere height, the structure function becomes proportional to the path length squared. Since the structure function is an average squared delay difference, the rss delay difference between the two antennas will be approximately proportional to (path length)$^{0.5}$ for distances less than the troposphere height and to (path length)$^{1.0}$ for distances greater than the troposphere height. This result is consistent with the intuitive picture that many small irregularities contribute to the short distance structure while a small number of larger irregularities dominate the large distance structure.

The second assumption of the fluctuation model outlined here is that temporal fluctuations are caused by spatial fluctuations which are moved past a site by the wind. The persistence of this "frozen" spatial structure (Ref. 11) allows the calculation of temporal structure functions by replacing $\rho = vT$ in Eq. (4), where v is the wind speed and T is the time at which the structure function is to be evaluated. In other words, the temporal structure function

$$\bar{D}_{\tau,\theta,\phi}(T) = \langle(\tau_{\theta,\phi}(\vec{x}, t + T) - \tau_{\theta,\phi}(\vec{x}, t))^2\rangle$$

for a time interval T at a single station is equivalent to the spatial structure function $D_{\tau,\theta,\phi}(\rho)$ between two antennas separated by a distance $\rho = vT$. That is,

$$\bar{D}_{\tau,\theta,\phi}(T) = D_{\tau,\theta,\phi}(\rho)|_{\rho=vT} \qquad (5)$$

Thus, an interesting feature of Eq. (4) is that it describes not only the differential fluctuations between two antennas but the temporal fluctuations observed at a single antenna as well. Temporal structure functions therefore have the same curved shape as Fig. 1, and can be described by fitting a polynomial to Fig. 1, as detailed in Appendix A. In Eqs. (4) and (5), ϕ is the angle between the direction of the wind and the antenna line of sight projected on the surface of Earth.

Before discussing the effect of the above model assumptions and derivations on VLBI observables, it will be useful to assign values to the three free parameters implicit in Eqs. (4)

and (5): The effective wet troposphere height h, the wind speed v, and the structure function constant C. Except as noted, subsequent calculations assume h to be 2 km, which is the approximate scale height of the wet troposphere. The wind speed v is taken to be 8 m/s, representative of typical winds at 1-km altitude at Goldstone, California. It will be shown below that once h and v are specified, C can be calculated knowing the standard deviation of the zenith wet delay over any given time interval. The standard deviation can be determined either from VLBI estimates of the zenith parameter for individual experiments or from WVR data. To arrive at a value of C which represents average Goldstone water vapor conditions, we will use WVR data taken at the Mojave station over a period of years. As noted below, C derived in this way is 1.99×10^{-7} m$^{1/3}$.

III. The Effect of Water Vapor Fluctuations on VLBI Observables

The fluctuating water vapor refractivity will cause errors in the delay and delay rate VLBI observables. In order to assess the average magnitude of the delay error, the variance of the water vapor delay fluctuation for arbitrary antenna orientation will be written as a function of observation time interval. We use the variance at zenith to calculate the structure function normalization constant C. The Allan standard deviation of the fluctuations is then presented to indicate the effect of the fluctuations on the delay rate observable. At the end of this section, the observable elevation dependence for selected time scales will be presented and compared to elevation signatures in the DSN VLBI data set.

The variance of the delay at a single station along the raypath with elevation θ and a projected angle ϕ with respect to the wind is given by

$$\sigma^2_{\tau,\theta,\phi}(T) = (1/T)^2 \int_0^T (T-t)\, \overline{D}_{\tau,\theta,\phi}(t)\, dt \qquad (6)$$

Equation (6) is derived in Appendix B. The constant C enters in Eq. (6) through $\overline{D}_{\tau,\theta,\phi}(T)$ as in Eq. (5). Standard deviations of WVR data taken at Goldstone over a several year period show that $\sigma_{\tau,0,0}(T)|_{T=24 \text{ hours}}$ is 1.67 ±0.73 cm of delay (Ref. 12). The Goldstone result applied to Eq. (6) yields a value of $C = 1.99 \times 10^{-7}$ m$^{-1/3}$. The standard deviation of the zenith delay is shown versus time interval in Fig. 2 along with the standard deviation for $\theta = 90°$ and $(\theta, \phi) = (20°, 45°)$. Again, the model describes a curved rather than power law shape. Over very small time intervals, the standard deviation is proportional to $T^{5/6}$; over very large intervals, it is proportional to $T^{1/3}$. The elevation dependence also exhibits the same qualitative feature as it did for the square root of the structure function calculated above.

The Allan variance is a relatively good approximation to the delay rate variance and is therefore calculated in terms of the structure function in Appendix B. The result is the simple formula

$$A_{\tau,\theta,\phi}(T) = (4\overline{D}_{\tau,\theta,\phi}(T) - \overline{D}_{\tau,\theta,\phi}(2T))/(2T^2) \qquad (7)$$

The Allan standard deviation, which is the square root of Eq. (7), is shown in Fig. 3 for the same angle combinations as in Figs. 1 and 2. The curved spectrum which maps more strongly with elevation at large time scales than at small is evident again in the Allan standard deviation. The Allan standard deviation is proportional to $T^{-1/6}$ at short time intervals and $T^{-2/3}$ at large time intervals. For reference, the hydrogen maser Allan standard deviation is also shown in Fig. 3.

To compare observable model predictions to VLBI data, delay and delay rate elevation dependences for specified time intervals are presented below. VLBI analysts are typically concerned with delay fluctuations on the order of a few hours if zenith delays are statistically estimated. In that case, fluctuations on longer time scales are largely absorbed by troposphere parameters in the least squares solution. Plotted in Fig. 4(a) is the calculated standard deviation of tropospheric delay for a 3-h time period. The standard deviation is plotted versus the path length in zenith units. The dashed line in Fig. 4(a) shows the contribution of the mean thermal noise, called system noise (Ref. 3), for the DSN VLBI data set. According to this figure, system noise on the average is a more severe error source than that due to water vapor fluctuation. The main conclusion from Fig. 4(a) is that if the parameterization of the troposphere presented here is realistic, the delays of the DSN data set are not currently dominated by the dynamic wet troposphere.

Figure 4(b) shows the Allan standard deviation as calculated from the model for a typical DSN scan length time of 200 s, versus the path length in zenith units. Because the delay rate observables is the average rate of change of delay over a 200-s scan length, the Allan standard deviation at that time interval is close to the delay rate scatter. The dashed line on Fig. 4(b) shows the estimated Allan standard deviation due to instrumental phase instability as measured at DSS 13.[2] Instrumental phase instability due to amplification and heterodyning is believed to be the largest non-atmospheric error in

[2]Edwards, C. D., IOM 335.4-473 to Tracking Systems and Applications Section, Jet Propulsion Laboratory, February 1985.

the delay rate measurement; for example, it is approximately an order of magnitude larger than the error due to the hydrogen maser clock. According to the model, with the atmospheric parameters of Section II, the delay rate observable error, unlike the delay error, is dominated by the dynamic wet troposphere.

To test the above conclusions, Figs. 5(a) and 5(b) show the rss delay and delay rate residuals from the DSN VLBI data set as a function of the sum of the path lengths for the raypaths of an observation. The figures are based on 1978–1985 VLBI data taken on the California–Spain and California–Australia baselines. In agreement with the above model considerations, the delay residuals of Fig. 5(a) show no trend with path length. For the delay rates in Fig. 5(b), however, there is a significant increase in rss residuals as the path length increases, much like the model result of Fig. 4(b). The solid line represents the curve in Fig. 4(b), increased 30% with an overall scaling factor. The shape of the model curve is in agreement with the VLBI data. The underestimation of the normalization of the model curve by 30% is in part due to uncertainties in normalization parameters and in part to the tendency of the Allan standard deviation to underestimate the delay rate scatter. In the future, we plan to calculate the delay rate temporal standard deviation, which could be directly compared with the data and perhaps alleviate the need for most of the 30% scaling factor. Comparing Figs. 4 and 5 shows that the calculated levels of wet tropospheric disturbance are in approximate agreement with the levels observed in the DSN VLBI data set. In the case of the delay rate observable, the calculated path length dependence is also consistent with the data.

It should also be noted from Fig. 5(a) that if the DSN noise levels can be reduced below 1–2 cm per observation, the VLBI errors will be dominated in both delay and delay rate by the fluctuating wet troposphere. Dry tropospheric inhomogeneities may also become important. When, for example, DSS 13 is instrumented with a Mark III data acquisition system in the next year, 1–2 cm noise levels should be attainable on most sources. Because of the magnitude of the delay and delay rate tropospheric effects indicated by Figs. 4 and 5, the delay rate observable is usually down-weighted relative to the delay in VLBI analysis. Since the delay observable is therefore much more important in the parameter estimation procedure than the delay rate, the lower noise levels available with improved instrumentation will allow a more thorough empirical study of tropospheric effects on the entire VLBI solution.

In the model calculations in this section, the wet troposphere effective height h, wind speed v, and normalization constant C were assigned the values given at the end of Section II. Below we give the dependence of the delay and Allan standard deviations (Eqs. 6 and 7) on h, v, and C. Numerical analyses of Eqs. (4), (6), and (7) imply that the delay standard deviation is proportional to $Chv^{1/3}$ for $T \gg 250$ s. The Allan standard deviation at 200-s time intervals is proportional to $Ch^{0.7}\ v^{0.6}$. These approximate relations can be used to coarsely gauge the dependence of the statistical quantities on the properties of the frozen-in wet troposphere.

IV. The Effect of Water Vapor Fluctuations on VLBI Parameter Estimates

The effect of the dynamic wet troposphere on the delay and delay rate observables ultimately corrupts the determination of geometric parameters in the VLBI estimation procedure. As mentioned in the introduction, the geometric parameters of baseline and source position define the radio reference frame relative to which spacecraft are navigated. The model presented in previous sections leads to a calculation of the covariance of any two parameters due to the dynamic wet troposphere. Along with the aforementioned model parameters, such as wind speed and the overall normalizing constant, the particular VLBI observing schedule is needed.

In VLBI, parameters are usually estimated by a linear least squares procedure. The parameter estimates to be discussed are actually corrections to *a priori* values. These estimates can be expressed as linear functions of the delay and delay rate observables. They will be expressed below as a function of the delay observable only, because the delay observable dominates the VLBI solution. In the least squares analysis, the ith parameter P_i is calculated as a linear combination of the observables. It is given by

$$P_i = \sum_k F_{i,k}\,(\tau_{2k} - \tau_{1k}) \tag{8}$$

where $F_{i,k}$ are the observing schedule dependent coefficients generated by the least squares process which multiply the kth observable in the summation for the ith parameter. The $\tau_{m,k}$'s are the delays experienced by the wave arriving at the mth station for the kth observation. In this treatment, the statistical variation of the $\tau_{m,k}$'s are assumed to be due only to the dynamic wet troposphere. From Eq. (8) follows the expression for the parameter covariance between the ith and the jth parameters.

$$\langle (P_i - \langle P_i \rangle)(P_j - \langle P_j \rangle) \rangle = \sum_k \sum_l F_{ik} F_{jl}$$

$$[\mathrm{cov}(\tau_{2k}, \tau_{2l}) + \mathrm{cov}(\tau_{1k}, \tau_{1l})] \tag{9}$$

where

$$\mathrm{cov}(\tau_{mk}, \tau_{ml}) = \langle (\tau_{mk} - \langle \tau_{mk} \rangle)(\tau_{ml} - \langle \tau_{ml} \rangle) \rangle \quad (10)$$

It has been assumed in Eq. (9) that the stations are far enough apart that their tropospheres are uncorrelated. The brackets refer to the same ensemble average as in Eq. (1), where each ensemble member consists of a value of the randomly varying refractivity for each point in space.

The frozen-in statistical model described above allows for the calculation of the covariance of Eq. (10). Substituting the expression in Appendix A, Eq. (A-1), into Eq. (10) and using the relation Eq. (A-3), yields the result

$$\mathrm{cov}(\tau_k, \tau_l) = (1/\sin\theta_k)(1/\sin\theta_l)\left[h^2 \sigma_n^2 - \frac{1}{2}\int_0^h \int_0^h D_n(|(\vec{\mathbf{r}}_k(z) - \vec{\mathbf{v}}t_k) - (\vec{\mathbf{r}}_l(z') - \vec{\mathbf{v}}t_l)|)\, dz\, dz'\right] \quad (11)$$

where the station index has been suppressed and σ_n^2 is the variance of wet refractivity fluctuations. It is given by

$$\sigma_n^2 = \langle n(\vec{\mathbf{r}})^2 \rangle - \langle n(\vec{\mathbf{r}}) \rangle^2 \quad (12)$$

where the $n(\vec{\mathbf{r}})$ and $D_n(r)$ functions are as in Eq. (2), and θ_k and θ_l are the elevation angles for the kth and lth observations. $\langle n(\vec{\mathbf{r}}) \rangle$ and $\langle n(\vec{\mathbf{r}})^2 \rangle$ are independent of $\vec{\mathbf{r}}$ in the homogeneous picture of the atmosphere. The times t_k and t_l correspond to the kth and lth observations, and $\vec{\mathbf{r}}_k(z)$ and $\vec{\mathbf{r}}_l(z')$ describe the point in space associated with the kth and lth lines of sight at heights z and z', respectively. The wind velocity in Eq. (11) is assumed to be independent of scan number. Within the framework of this model, Eq. (11) is the covariance of the wet tropospheric delay for observations along any two rays separated by arbitrary times.

Substituting Eq. (11) into Eq. (10) and Eq. (10) into Eq. (9) yields the complete expression for the VLBI parameter covariances. We write it below with the modification that the actual curvature of Earth be considered in describing the mapping of a zenith path length to arbitrary elevation angles (Ref. 13):

$$\left.\begin{aligned}\mathrm{cov}(P_i, P_j) = \sum_k \sum_l F_{ik} F_{jl} \Big[& m_k m_l h^2 \sigma_n^2 \\ & - (2 \sin\theta_k \sin\theta_l)^{-1} \int_0^{h'_k} \int_0^{h'_l} dz\, dz'\, D_n(s) \Big]\end{aligned}\right\} \quad (13)$$

where

$$s^2 = (z \cot\theta_k \cos\phi_k - z' \cot\theta_l \cos\phi_l - v(t_k - t_l))^2 + (z \cot\theta_k \sin\phi_k - z' \cot\theta_l \sin\phi_l)^2 + (z - z')^2$$

where m_k and m_l are the actual mapping from zenith to the lines of sight at θ_k and θ_l, respectively. h'_k is $h\, m_k \sin\theta_k$ and h'_l is $h\, m_l \sin\theta_l$. The wind vector is along the x axis and ϕ_k and ϕ_l are the azimuths of the kth and lth scan relative to the wind vector direction.

Before giving a sample parameter covariance result, it is important to clarify the meaning of the σ_n^2 term in Eqs. (11), (12), and (13). To get a finite ensemble averaged value for σ_n^2, the troposphere must be completely uncorrelated at points infinitely distant from each other. Then

$$\sigma_n^2 = (1/2) D_n(\infty) \quad (14)$$

from the definition of the structure function in Eq. (1) and the assumption of homogeneity. The structure function of Eq. (2) does not converge at infinity, and this unphysical feature of the Kolmogorov structure function must be altered. A phenomenological function must be used which takes the form of Eq. (2) for small distances and converges to a constant at $r = \infty$. We choose the modified structure function to be

$$D'_n(R) = C^2 R^{2/3} / [(1 + (R/L)^{2/3}] \quad (15)$$

where L is a saturation scale length. L is chosen to be 2000 km to be in approximate agreement with Ref. 11. This value of L also produces reasonable very long term rms tropospheric variations of about 3.5 cm, consistent with the total tropospheric fluctuation over many months at mid-latitudes. In actual calculations, $D'_n(R)$ must be substituted into Eq. (13) in place of $D_n(R)$ to calculate parameter covariances. It will be demonstrated below that the actual covariances calculated for geometric parameters are very insensitive to the choice of L, provided L is in a physically reasonable range.

Figure 6 shows the baseline length error as calculated by Eqs. (13), (14), and (15) as a function of time over which troposphere zenith parameters are estimated in the VLBI analysis. The experiment was conducted in May 1983 on the

California–Australia baseline. Two different sets of constants were used in the plot with the constraint that the daily zenith delay standard deviation be 1.67 cm. As noted, the wind speed was assumed to be 8 and 2 m/s. In each case the daily zenith constraint was met by adjusting C to the value of 1.99×10^{-7} and 3.19×10^{-7}, respectively. Figure 6 shows by the similarity of the two curves that the baseline length covariances calculated are sensitive mainly to the zenith standard deviation. The covariances shown in Fig. 6 are insensitive to changing the more uncertain parameters of troposphere height, refractivity structure function normalization, or the wind speed. A similar statement can be made about the choice of the scale distance L. To test the length error sensitivity to h, h was changed from 2 km to 1 km and L varied between 3000 km to 1000 km; no appreciable change in the length error calculation resulted in either case.

Figure 6 also allows the determination of the optimal number of troposphere parameters for a given VLBI schedule. The figure shows that baseline length errors for the experiment considered can be reduced from the 5-cm to the 3-cm range if the length of time for the zenith solution is less than approximately 4 h. Estimating the zenith more frequently than every 2 h, however, does not reduce the length error much below the 3.5-cm level. Figure 6 is only an example of how the model presented here can be used to calculate VLBI parameter errors. The estimate of baseline length errors varies with observing schedule as well as with the troposphere fluctuation normalization, which can be approximated from the fluctuation of the VLBI estimated troposphere parameters.

Equations (11) through (15) also suggest a possible refinement to the VLBI parameter estimation procedure. Most VLBI estimation schemes currently in use do not allow for a correlation between observations, because system noise is in principle uncorrelated from time to time. But the troposphere noise is correlated, as is evidenced, for example, by the shape of the delay standard deviation calculated in Section III. If the model outlined provides a sufficiently accurate description of the troposphere-induced delays, then Eq. (11) evaluated with D'_n as given in Eq. (15) can be used in the least squares analysis. This expression for the observable covariance could be used in the observable covariance matrix in the VLBI parameter estimation routines. Work is in progress at JPL to modify the MASTERFIT parameter estimation software to include these off-diagonal elements in the covariance matrix. At present, it is not known whether the inclusion of the troposphere covariance will be adopted as a standard procedure because of the large computer resources needed to compute the covariance of Eq. (11). We will either include the results of calculations based on Eq. (11) or simply calculate the parameter errors caused by the troposphere in the current estimation scheme using Eq. (13) with D'_n.

V. Model Validation

The above model description rests on the two aforementioned physically appealing but simplified assumptions about frozen-in turbulence. Here we compare the salient results of the model to published results. Comparisons between model calculations and spatial structure function results are followed by comparisons with Allan standard deviations and power spectra. At the end of this section, the question of the altitude independence of C and the wind vector is discussed.

Spatial structure functions $D_{\tau,\theta,\phi}(\rho)$ were measured by Armstrong and Sramek (Ref. 14) at the Very Large Array. For each ρ, θ and ϕ were averaged over many observations. Armstrong and Sramek fit their structure functions to power laws and found powers between 0.84 and 1.95 with an average of 1.4. Plotted in Fig. 7 are the exponents from local power law fits to the calculated structure functions of Fig. 1, as a function of α. Assuming a troposphere height of 2 km and taking the average ρ of Ref. 14 to be about 3 km yields an expected average exponent between 0.95 and 1.35 corresponding to the zenith and 20-deg elevation prediction from the model. The exact model value depends on the elevation angle spread of the actual experiment. Thus, the model qualitatively agrees with the data, slightly underestimating the measured slope. There is some indication in the figures of Ref. 14 that the structure function does curve at large ρ, but the evidence is not conclusive.

In Ref. 11, Dravskikh and Finkelstein describe a structure function which conforms to the atmospheric data they have studied. They state that the data are consistent with a structure function made up of two power laws. The function is proportional to $\rho^{5/3}$ for spatial scales less than 5.6 km, and proportional to $\rho^{2/3}$ for scales larger than 5.6 km. The asymptotic power law exponents agree with our model calculation. For a troposphere height of 2 km, the point where the power laws change would be at $\alpha = 2.8$. Such a change could easily be imagined to take place at this value of α in Fig. 1, if one were trying to fit the model result of Fig. 1 to a two-component power law. Although the agreement with our model is very good, it should be noted that Dravskikh and Finkelstein do not clearly describe the origin of either their data or their model assumptions.

The Allan standard deviation of VLBI phase fluctuations, presumably due to the wet troposphere, $A_{\tau,\theta,\phi}(T)$, was measured by Rogers et al. in Ref. 15. It is of the same order of magnitude as that shown in Fig. 3, but, more importantly, it is clearly curved. The curvature is not as extreme as the model predicts. This could be in part due to system noise contributions to the Allan standard deviation at very short time scales as well as to inadequacies in the above model.

Tropospheric temporal power spectra measured with a WVR by Hogg et al. (Ref. 16) exhibit nearly power law behavior with an exponent of roughly 1.75, corresponding to an Allan standard deviation slope of −0.625 (see Ref. 9 and Eq. 7). This is close to the model prediction behavior for long time scales, but there is no evidence of the curved shape predicted by the model at short time scales. Again, either instrumental noise or inadequacies in the above model could be responsible for the discrepancies between the model and the published data.

Power spectra measured by Thompson et al. (Ref. 17) show more of a curved shape as expected from the above discussion. At high frequencies near 0.1 Hz, the power law exponent for the power spectrum shown is near −2.86. Near the low frequency of 0.01 Hz, the exponent is approximately −1.92. These two slopes correspond to short- and long-term Allan standard deviation slopes of −0.07 and −0.54, respectively, in qualitative agreement with model predictions.

A summary of the power law exponents from model predictions and data is presented for the discussed statistical quantities in Table 1. The table shows a list of statistical quantities in the first column and the mathematical expression used in the text in the second. The third column shows the exponent of the independent variable describing local power law fits for small and large scales of the variable, connected by an arrow. For distance, small means much less than the water vapor scale height (~2 km). Large scales mean distances much greater than the scale height. Small and large time scales correspond to the small and large distance scales divided by the average wind speed. The fourth column shows the power laws determined from measurements, with small and large scales noted as before, if available from the data. The fifth column shows the reference for the data quoted in the fourth column.

Investigations of the range of validity of the above calculations will have to address the validity of the homogeneity ascribed to the constant C and the wind vector. Measurements of C (Ref. 18) show varying altitude dependencies. The insensitivity to the effective height h discussed in Section IV and calculations with an exponentially decreasing C suggest the adequacy of the slab model used in this article for most applications. Data on the wind vector (Ref. 19) also show a variety of altitude dependences. Again, some average wind speed present over an average height may suffice, but this must be investigated. In the worst case, the equations for the wet tropospheric effects on observables and parameters could be modified to include altitude dependences for C and the wind speed, at the cost of calculational complexity.

The model qualitatively agrees with the references cited; however, more experiments are needed to really test the limitations of the model. To that end, we have conducted a set of WVR experiments with simultaneous wind vector monitoring at Goldstone. The data are currently being analyzed and will be reported in the near future.

VI. Conclusions and Discussion

The description of water vapor fluctuations based on frozen-in Kolmogorov turbulence leads to estimates of the effect of the dynamic wet troposphere on VLBI observables and parameters. Based on this description, one finds that the current DSN VLBI data set errors are troposphere-dominated for delay rates only. Since parameters are largely determined by the delay observables, formal errors in the 1978–1985 DSN VLBI data set do not have to be substantially modified to account for the dynamic wet troposphere.

Estimated parameter covariances were derived within the framework of the statistical model. A sample calculation of baseline length errors for one of the DSN California–Australia experiments showed the capability of repeated zenith parameter estimation to reduce baseline length error. The example showed that, under typical observing conditions, troposphere-induced baseline length error could be reduced from 5 cm to 3 cm as the estimation time for zenith delay was decrased.

All estimates of observable and parameter effects in this article are dependent upon normalization to the Goldstone WVR data, as mentioned in Section III. The spread of the measured daily zenith standard deviations mentioned in Section III is about 40% of the nominal 1.67 cm used throughout the article. This is a good indication of how much quoted numbers can vary over time at a particular site. As has been mentioned, it may be possible to use VLBI or WVR data to obtain zenith standard deviations and normalize the statistics for individual experiments. The reliability of that procedure is being checked with the recent WVR data taken at Goldstone.

Our future efforts include the analysis of several WVR experiments performed in the last few months, which should help to resolve the limitations of the model. These experiments should also prove useful in assessing the character of the noise contribution of the WVR instruments. The practical benefits of putting the calculated troposphere covariance into the JPL VLBI parameter estimation scheme will be studied with a test version of MASTERFIT. VLBI data will then be processed with the troposphere covariance and the results compared to processing with WVR measurements.

Acknowledgment

We would like to acknowledge O. J. Sovers for analyses of the DSN VLBI data set used in this article.

References

1. Gold, T., "Radio Method for the Precise Measurement of the Rotation Period of the Earth," *Science*, Vol. 157, pp. 302–304, July 1967.

2. Rogers, A. E. E., "Very Long Baseline Interferometry with Large Effective Bandwidth for Phase-Delay Measurements, *Radio Science*, Vol. 5, pp. 1239–1247, October 1970.

3. Thomas, J. B., *An Analysis of Long Baseline Radio Interferometry*, Technical Report 32–1526, Vol. VII, Jet Propulsion Laboratory, Pasadena, Calif., pp 37–50, 1972.

4. Hinder, R. A., "Observations of Atmospheric Turbulence with a Radio Telescope at 5 GHz," *Nature*, Vol. 225, pp. 614–617, February 1970.

5. Treuhaft, R. N., Lanyi, G. E., and Sovers, O. J., "The Dynamic Wet Troposphere Error Budget for Intercontinental VLBI," *Transactions, American Geophysical Union (EOS)*, Vol. 66, p. 858, November 1985.

6. Sovers, O. J., Thomas, J. B., Fanselow, J. L., Cohen, E. J., Purcell Jr., G. H., Rogstad, D. H., Skjerve, L. J., and Spitzmesser, D. J., "Radio Interferometric Determination of Intercontinental Baselines and Earth Orientation Utilizing Deep Space Network Antennas: 1971 to 1980," *Journal of Geophysical Research*, Vol. 89, pp. 7597–7607, September 1984.

7. Shapiro, I. I., "Estimation of Astrometric and Geodetic Parameters from VLBI Observations," in *Methods of Experimental Physics*, M. L. Meeks, Ed., New York: Academic Press, pp. 261–276, 1976.

8. Resch, G. M., Hogg, D. E., and Napier, P. J., "Radiometric Correction of Atmospheric Path Length Fluctuations in Interferometric Experiments," *Radio Science*, Vol. 19, pp. 411–422, January 1984.

9. Tatarskii, V. I., *Wave Propagation in a Turbulent Medium*, New York: Dover, 1961.

10. Ishimaru, A., *Wave Propagation and Scattering in Random Media*, Vol. 2, New York: Academic Press, 1978.

11. Dravskikh, A. F., and Finkelstein, A. M., "Tropospheric Limitations in Phase and Frequency Coordinate Measurements in Astronomy," *Astrophysics and Space Science*, Vol. 60, pp. 251–265, 1979.

12. NASA Crustal Dynamics Data Information System, Goldstone Water Vapor Radiometer Data, 1981–1983.

13. Lanyi, G. E., "Tropospheric Delay Effects in Radio Interferometry," *TDA Progress Report 42–78*, pp. 152–159, Jet Propulsion Laboratory, Pasadena, Calif., 1984.

14. Armstrong, J. W., Sramek, R. A., "Observations of Tropospheric Phase Scintillations at 5 GHz on Vertical Paths," *Radio Science*, Vol. 17, pp. 1579–1586, November 1982.

15. Rogers, A. E. E., Moffet, A. T., Backer, D. C., and Moran, J. M., "Coherence Limits in VLBI Observations at 3-Millimeter Wavelength," *Radio Science*, Vol. 19, pp. 1552–1560, November 1984.

16. Hogg, D. C., Guiraud, F. O., and Sweezy, W. B., "The Short-Term Temporal Spectrum of Precipitable Water Vapor," *Science*, Vol. 213, p. 1112, September 1981.

17. Thompson, M. C., Wood, L. E., Janes, H. B., and Smith, D., "Phase and Amplitude Scintillations in the 10 to 40 GHz Band," *IEEE Transactions on Antennas and Propagation*, AP-23, pp. 792–797, November 1975.

18. Thompson, Jr., M. C., Marler, F. E., and Allen, K. C., "Measurement of the Microwave Structure Constant Profile," *IEEE Transactions on Antennas and Propagation*, AP-28, pp. 278–280, March 1980.

19. Chadwick, R. B., Moran, K. P., Strauch, R. G., Morrison, G. E., and Campbell, W. C., "Microwave Radar Wind Measurements in the Clear Air," *Radio Science*, Vol. 11, pp. 795–802, October 1976.

Table 1. Comparison of behavior of calculated and measured tropospheric statistics

Statistic	Expression from text	Power law exponent		
		This model	Data	Reference for data
Spatial structure function	$D_{\tau,\theta,\phi}(\rho)$ Eq. (4)	$5/3 \rightarrow 2/3$	1.4 $5/3 \rightarrow 2/3$	Ref. 14 Ref. 11
Temporal structure function	$\bar{D}_{\tau,\theta,\phi}(T)$ Eq. (5)	$5/3 \rightarrow 2/3$	– – –	– – –
Standard deviation of zenith display	$\sigma_{\tau,\theta,\phi}(T)$ Eq. (6)	$5/6 \rightarrow 1/3$	– – –	– – –
Allan standard deviation	$\sqrt{A_{\tau,\theta,\phi}(T)}$ Eq. (7)	$-1/6 \rightarrow -2/3$	$-0.25 \rightarrow -0.50$ -0.63 $-0.07 \rightarrow -0.54$	Ref. 15 Ref. 16 Ref. 17

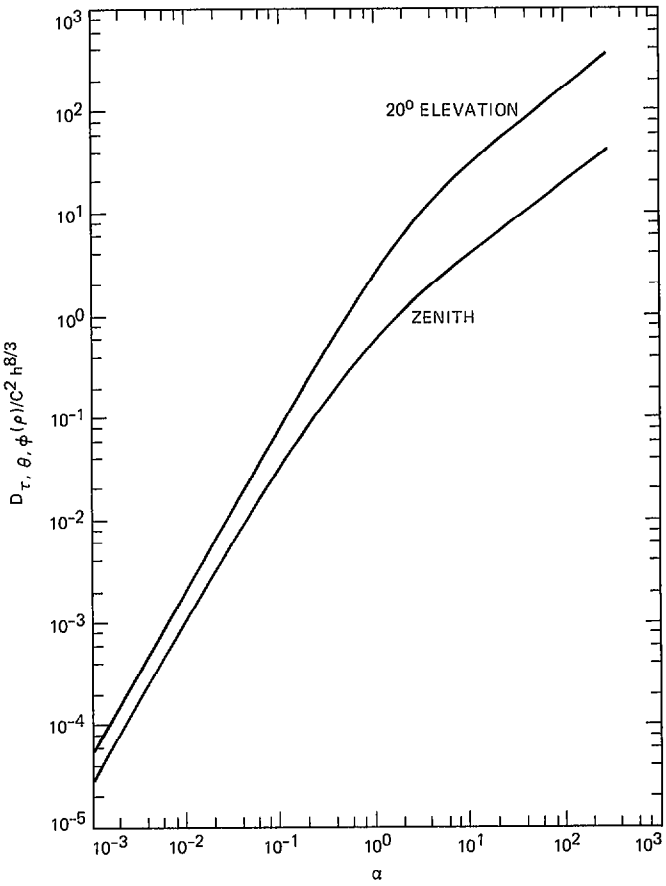

Fig. 1. The spatial structure function, calculated from Eq. (4) normalized to $C^2 h^{8/3}$, as a function of $\propto = \rho/h$, where ρ is the distance between two points on Earth at which the wave is received, and h is the effective height of the wet troposphere. Curves are shown for $(\theta,\phi) = (90°,0°)$ and $(\theta,\phi) = (20°,45°)$.

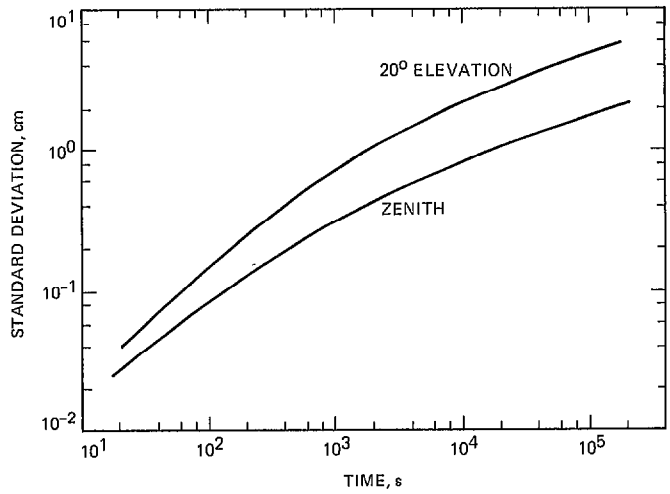

Fig. 2. The single-site, calculated standard deviation of the delay fluctuation as a function of time interval. The standard deviation is shown for zenith and 20-deg elevation. Refractivity structure function normalization, wet troposphere height, and wind speed are as noted at the end of Section II.

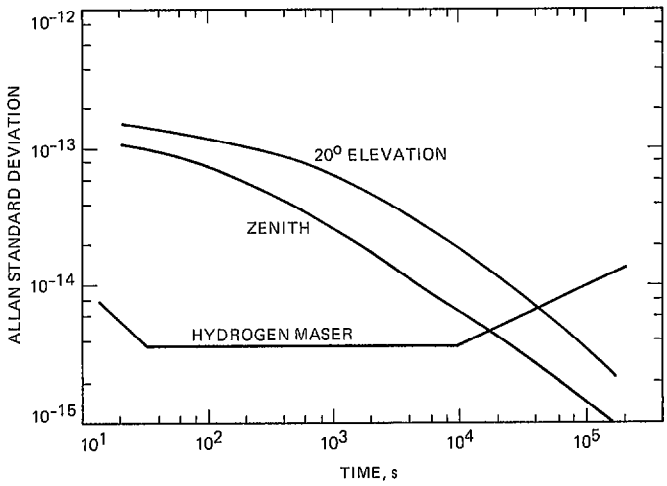

Fig. 3. The single-site, calculated Allan standard deviation of the delay fluctuation as a function of time interval. The Allan standard deviation is shown for zenith and 20-deg elevation.

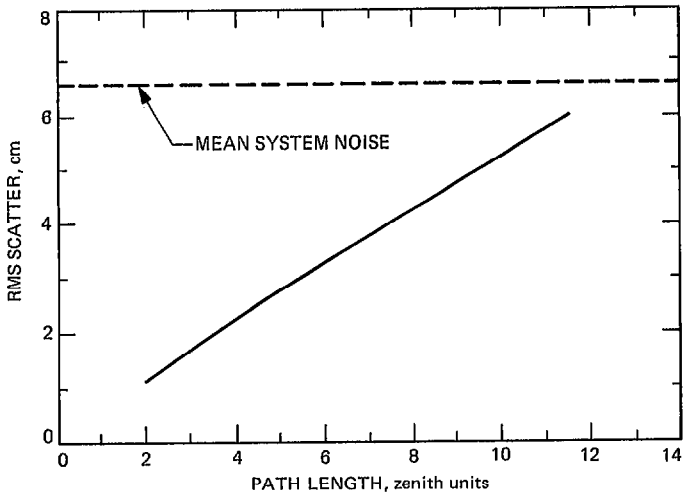

Fig. 4(a). The calculated delay standard deviation at a 3-h time interval as a function of total path length for two raypaths through the atmosphere for a VLBI observation. The dashed line is the mean system noise for the 1978–1985 DSN VLBI data set.

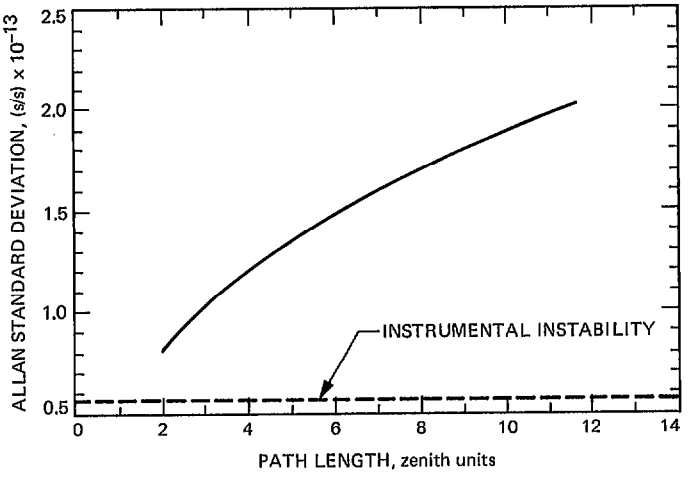

Fig. 4(b). The calculated delay Allan standard deviation at a 200-s time interval as a function of path length for two raypaths for a VLBI observation. The dashed line is an estimate of the current instrumental instability as measured at DSS 13.

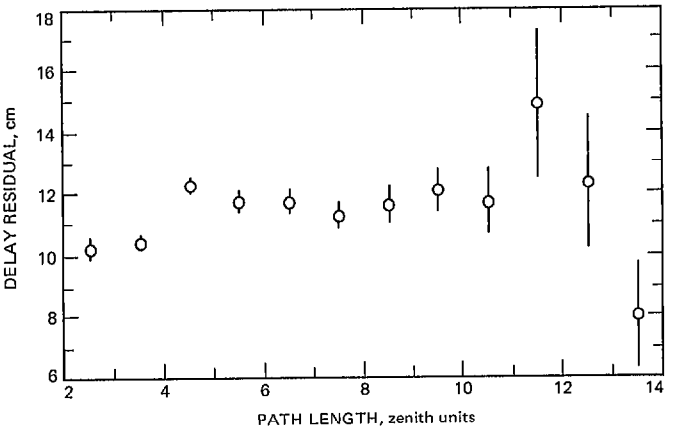

Fig. 5(a). The rms delay residual from the 1978–1985 DSN VLBI data set, for intercontinental observations only, versus path length through the atmosphere.

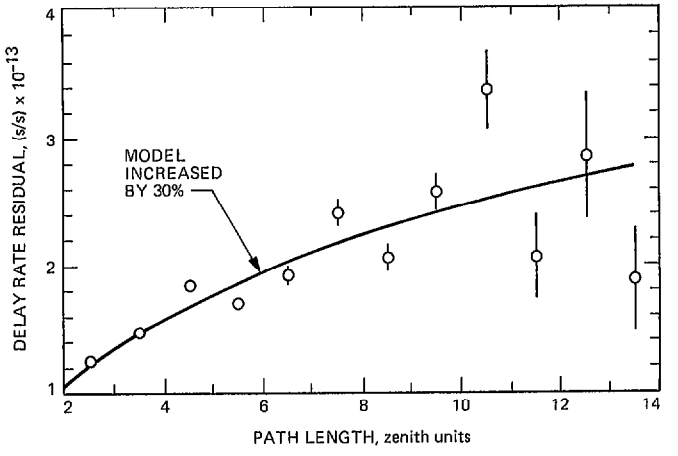

Fig. 5(b). The rms delay rate residual from the 1978–1985 DSN VLBI data set, for intercontinental observations only, versus path length through the atmosphere. The solid curve is the model prediction of Fig. 4(b) increased by 30%.

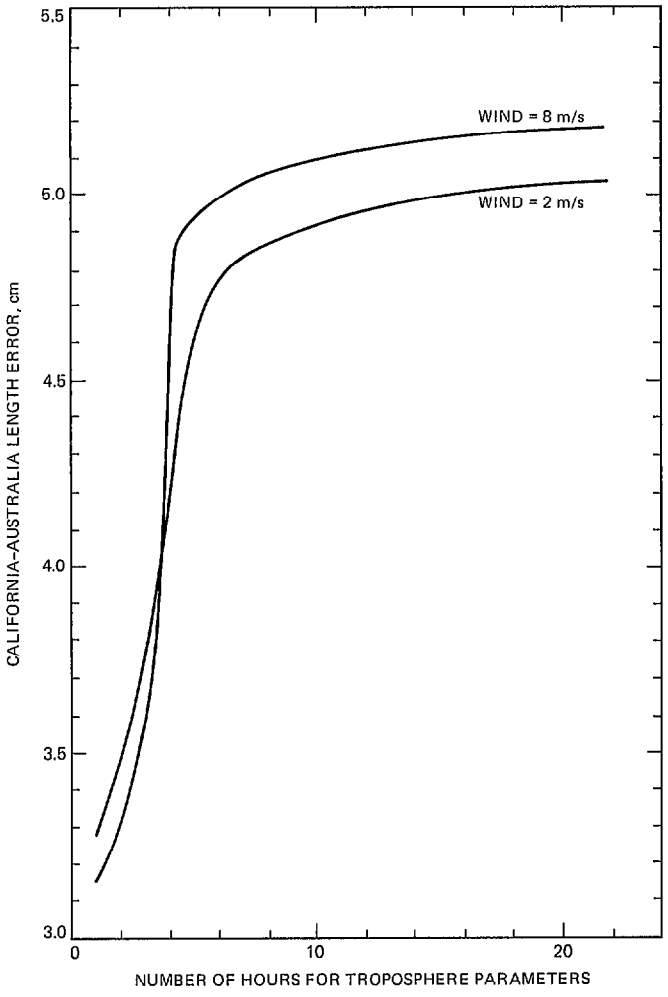

Fig. 6. The calculated California–Australia baseline length error as a function of the time over which zenith troposphere parameters are solved. Two curves are shown, one in which the wind speed was assumed to be the standard 8 m/s, and one in which the wind speed was assumed to be 2 m/s. For both curves the daily zenith standard deviation was taken to be 1.67 cm.

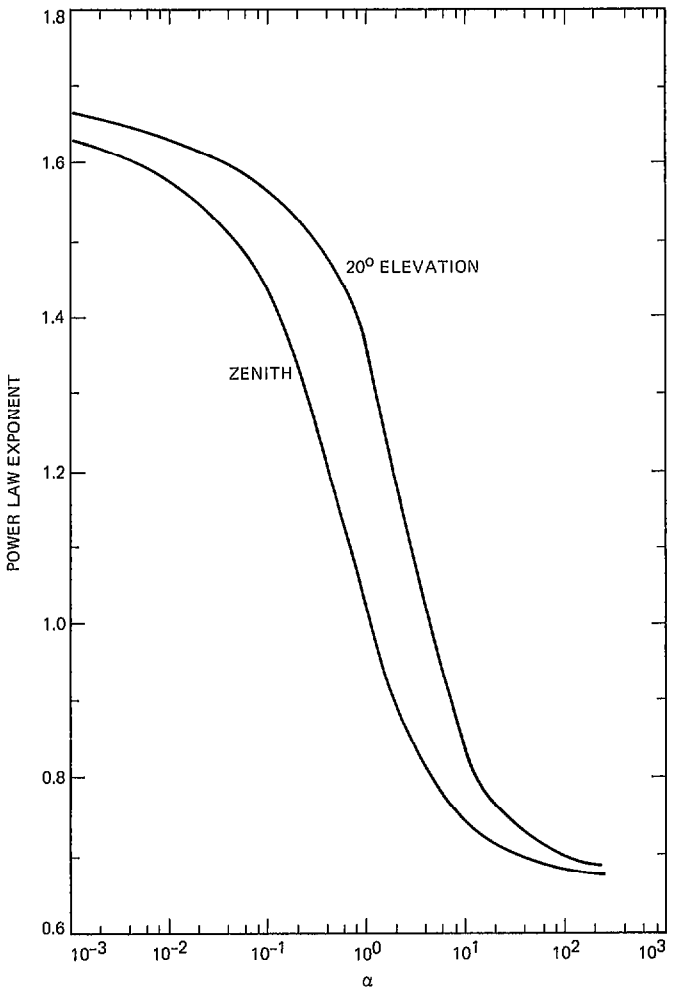

Fig. 7. Exponents from local power law fits to the curves in Fig. 1 versus α, where $\alpha = \rho/h$.

Appendix A

The Spatial Structure Function

The spatial structure function for the delay of waves propagating through the atmosphere to Earth is defined by Eq. (3). In order to derive the result of Eq. (4) for arbitrary lines of sight separated by a distance ρ, Earth will be considered flat. This will result in less than a 5% error at 6-deg elevation. Let $\tau_{\theta,\phi}(\vec{x})$ be the tropospheric delay experienced by a wave incident at a point on the Earth's surface $\vec{x}$. The wave arrives along the line of sight with elevation θ and azimuth ϕ.

Assuming geometric optics holds, $\tau_{\theta,\phi}(\vec{x})$ can be expressed as an integral of the refractivity along the raypath, as in Section II,

$$\tau_{\theta,\phi}(\vec{x}) = (1/\sin\theta)\int_0^h n(\vec{x} + \vec{r}(\theta, \phi, z))\, dz \quad \text{(A-1)}$$

where $n(\vec{x} + \vec{r}(\theta, \phi, z))$ is the refractivity evaluated at height z along the raypath originating at $\vec{x}$ and extending along the vector $\vec{r}$ with elevation and azimuth of θ and ϕ. The spatial structure function is

$$D_{\tau,\theta,\phi}(\rho) = \langle (\tau_{\theta,\phi}(\vec{x} + \vec{\rho}) - \tau_{\theta,\phi}(\vec{x}))^2 \rangle \quad \text{(A-2)}$$

To calculate the structure function of Eq. (4), the following relation is used: For any two arbitrary vectors $\vec{x}_1$ and $\vec{x}_2$, where $r = |\vec{x}_1 - \vec{x}_2|$,

$$D_n(r) = D_n(\vec{x}_1, \vec{x}_2) = 2\langle n^2 \rangle - 2\langle n(\vec{x}_1)\, n(\vec{x}_2) \rangle \quad \text{(A-3)}$$

Equation (A-3) follows from the definition of the structure function and the assumption mentioned in the text that the structure function of n depends only on the magnitude of the vector difference of its arguments. This assumption also implies that $\langle n^2 \rangle$ is independent of spatial coordinates. Substituting Eq. (A-1) into Eq. (A-2) and using Eq. (A-3) yields Eq. (4) in the text.

Since most of the quantities calculated in this article depend on the form of the spatial structure function of Fig. 1, parameters describing a polynomial fit to the curve of Fig. 1 are shown in Table A-1. The parameterization is as follows:

$$\log D_{\tau,\theta,\phi}(\alpha) = \sum_i a_i (\log \alpha)^i \quad \text{(A-4)}$$

where $\alpha = \rho/h$ and $D_{\tau,\theta,\phi}(\alpha)$ has been normalized to $C^2 h^{8/3}$. The a_i parameters are given in Table A-1.

Table A-1. Parameters from fit to numerical integration of spatial structure function

Parameter	Theta = 90	Theta = 20
0	-0.22318D+00	0.43292D+00
1	0.10108D+01	0.13450D+01
2	-0.22470D+00	-0.23695D+00
3	0.25715D-01	-0.85416D-01
4	0.32032D-01	0.30830D-01
5	-0.44802D-02	0.26228D-01
6	-0.47644D-02	-0.35145D-02
7	0.43030D-03	-0.39578D-02
8	0.40255D-03	0.11101D-03
9	-0.16176D-04	0.22698D-03
10	-0.13693D-04	0.95718D-04

Appendix B

Calculating Standard Deviations and Allan Variances From Structure Functions

Consider a random function of time $f(t)$. The variance of $f(t)$ over a time T is

$$\sigma_f^2(T) = \langle (1/T) \int_0^T dt' \, [f(t') - (1/T) \int_0^T dt'' \, f(t'')]^2 \rangle \tag{B-1}$$

By squaring the indicated bracketed quantity in Eq. (B-1) and using the relation in Eq. (A-3), one arrives at the following expression:

$$\sigma_f^2(T) = (1/T^2) \int_0^T \int_0^T D_f(t, t')/2 \, dt \, dt' \tag{B-2}$$

Assuming, as always, that $D_f(t, t') = D_f(|t - t'|)$ allows the simplification of Eq. (B-2) as follows:

$$\sigma_f^2(T) = (1/T^2) \int_0^T (T - t) \, D_f(t) \, dt \tag{B-3}$$

as in Eq. (6).

To calculate the Allan variance, start from the following form of the definition of the Allan variance for the random delay function $f(t)$:

$$A(T) = \langle [(f(t + T) - f(t)) - (f(t) - f(t - T))]^2 \rangle / 2T^2 \tag{B-4}$$

where t is an arbitrary time. Squaring the indicated quantity in Eq. (B-4) and applying the relation in Eq. (A-3) to the random function f yields a result analogous to Eq. (7) in the text.